Coupling of 2DH-3D Hydrodynamic Numerical Models for Simulating Flow Around River Hydraulic Structures

F. Kilanehei, S.T.O. Naeeni and M.M. Namin

School of Civil Engineering, College of Engineering,
University of Tehran, P.O. Box 11365-4563, Tehran, Iran

Abstract: In this paper, flow around river hydraulic structures has been simulated numerically using an efficient coupled 2DH-3D hydrodynamic model. In practical studies, 2DH numerical models are broadly employed to simulate the free surface flows; however, application of 3D models is unavoidable in some cases such as flow around river hydraulic structures, due to the variation of flow characteristics in depth. In this research, a reach of a wide river channel containing some hydraulic structures has been considered. This reach has been simulated by a coupled 2DH-3D system that models the area surrounding the hydraulic structures three dimensionally and the rest of reach, two dimensionally. The proposed coupled system is a combination of a 2DH model and a full 3D one. Solution domains in the 2DH and 3D spaces are covered using triangular and prismatic elements, respectively. Both models implement the finite volume fractional step method to discretize the main equations. Comparison of the results of flow modeling around a bridge pier and a spur dike (typical river hydraulic structures), using the 3D and the coupled models in the same computational domain, with the experimental data shows good precision and considerable efficiency of the proposed coupled model.

Key words: Coupled model · Non-hydrostatic free surface flow · River hydraulic structures · Fractional step method · Unstructured mesh · Finite volume

INTRODUCTION

Many researchers have been conducted numerically to investigate the flow behavior in rivers during last decades. River flows can be simulated by 1D, 2D and 3D models. One dimensional models represent flow in channel by averaging the equations over a cross section, providing average flow velocity and water elevation in each channel section. Horizontal two dimensional flow models typically simulate flow in a channel by averaging governing equations over the depth, giving horizontal components of velocity and water depth in each element. Three dimensional models solve cell averaged governing equations and provide pressure and three velocity components within each element.

Bridge piers, bridge abutments and spur dikes are among most constructed hydraulic structures. With the development of two and three dimensional numerical modeling techniques, several studies have been carried out recently in order to describe and model the flow patterns around hydraulic structures. Chen and Li [1], Tingsanchali *et al.* [2], Molls and Chaudhry [3] and Molls *et al.* [4] have implemented 2DH models. The main part of river flows can be predicted quite satisfactorily by 2DH models, but the depth variation and secondary flow resulting from hydraulic structures is difficult to simulate by these type of models [5]. Therefore 3D numerical model needs to be considered for simulation purposes. In compare with 3D models, the 2DH models are best known for their Low computational cost.

Flow in open channel particularly around hydraulic structures, have been also simulated by applying 3D models. Mayerle *et al.* [6], Ouillon and Dartus [7], Tseng *et al.* [8], Kamil *et al.* [9], Kimura and Hosoda [10], Zhou [11], Salaheldin *et al.* [12], Roulund *et al.* [13], Nagata *et al.* [14], Xuelin *et al.* [15], Xuelin [16], MacCoy *et al.* [17] and Yazdi *et al.* [18] are among the researchers who have applied 3D models for simulating flow behavior around river structures.

Corresponding Author: Fouad Kilanehei, School of Civil Engineering, College of Engineering,
University of Tehran, P.O. Box 11365-4563, Tehran, Iran,
Tel: +98-9122815532, Fax: +98-21-66403808.

One of the most important assumptions in the development and application of three dimensional flow models is related to pressure term. In this regard pressure distribution can be assumed to be hydrostatic or non-hydrostatic. Due to the presence of a strong vertical component of the flow in the upstream face of the hydraulic structures, the assumption of hydrostatic pressure distribution is not valid. Therefore, it is necessary to simulate flow patterns near the hydraulic structures using full hydrodynamic 3D models.

To simulate a long river which categorized as a large water body, it is necessary to use an accurate numerical model with low computational cost. In recent years, coupled flow models have become more popular including coupling of 1D-2D and 2D-3D models. In the coupled models, the study area has been divided into two part and different modeling procedures applied according to the important hydrodynamic phenomena existing in each part. This different regions should be interact with each other in order to have an accurate prediction of flow characteristics. Miglio *et al.* [19], Fang-li *et al.* [20] and Mahjoob and Ghiassi [21] have applied coupled 1D-2D models for channel flow simulation. Few numerical studies have been reported in the literature to couple 2DH and 3D models mainly focused on marine environment. Namin and Falconer [22] proposed a 2DH-3D coupled model to facilitate positioning the 3D area in a portion of a larger 2DH domain and then solved the governing equations of hydrodynamic simultaneously. Zounemat-Kermani and Sabbagh-Yazdi [23] developed a 2D-3D coupled model to simulate deep currents in a marine system.

Figure 1 shows a reach of a river with placement of hydraulic structures. In the current study, the part with the hydraulic structures is called the "*Near Field*" and the rest of the reach the "*Far Field*". The flow behavior in the Far Field has been considered mostly well mixed and therefore can be modeled two-dimensionally while the one in the Near Field should be modeled three dimensionally. A combination of 2DH model for far field of river domain and full 3D model for near field of hydraulic structures will result in accurate and efficient computations. The purpose of this research is to present an efficient coupled 2DH-3D system for flow simulation around hydraulic structures located in long rivers.

Governing Equations

DH Depth Averaged Equations: Integrating the 3D RANS equations from the river bed to the free surface and neglecting the Coriolis and wind forces, the shallow water equations can be derived as
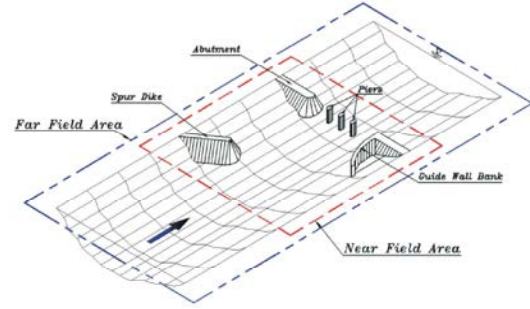

Fig. 1: Schematic view of Far and Near Fields in the vicinity of river hydraulic structures.

$$\frac{\partial \eta}{\partial t} + \frac{\partial p}{\partial x} + \frac{\partial q}{\partial y} = 0 \tag{1}$$

$$\frac{\partial p}{\partial t} + \frac{\partial (up)}{\partial x} + \frac{\partial (vp)}{\partial y} + gh\frac{\partial \eta}{\partial x} = \frac{\partial}{\partial x}(\vartheta_t^h \frac{\partial p}{\partial x}) + \frac{\partial}{\partial y}(\vartheta_t^h \frac{\partial p}{\partial y}) + \frac{1}{\rho}\tau_{bx} \tag{2}$$

$$\frac{\partial q}{\partial t} + \frac{\partial (uq)}{\partial x} + \frac{\partial (vq)}{\partial y} + gh\frac{\partial \eta}{\partial y} = \frac{\partial}{\partial x}(\vartheta_t^h \frac{\partial q}{\partial x}) + \frac{\partial}{\partial y}(\vartheta_t^h \frac{\partial q}{\partial y}) + \frac{1}{\rho}\tau_{by} \tag{3}$$

where h ($=\eta-z_b$) is the water depth; η is the free surface elevation; z_b is the bed elevation; u and v are the depth averaged velocity components in the x and y directions, respectively; p ($=uh$) and q ($=vh$) are the mass fluxes in the x and y directions, respectively; g is the gravitational acceleration; ρ is the fluid density; τ_{bx} and τ_{by} are respectively the bed shear stresses in x and y directions and ϑ_t^h is the eddy viscosity. Although the bed shear stress is a function of the near bed flow and not the mean flow, the following relations are applied adopted from the quadratic friction law

$$\tau_{bx} = \rho C_f u\sqrt{u^2+v^2} \tag{4}$$

$$\tau_{by} = \rho C_f v\sqrt{u^2+v^2} \tag{5}$$

where C_f is the dimensionless friction coefficient which can be expressed in terms of the Chezy coefficient C, Manning coefficient n or bed roughness height k_s as

$$C_f = \frac{g}{C^2} = \frac{g\,n^2}{h^{\frac{1}{3}}} = \frac{g}{(18\log(\frac{12h}{k_s}))^2} \tag{6}$$

In the present work, Smagorinsky model is employed to determine the eddy viscosity

$$\vartheta_t^h = (C_s\Delta)^2 \left|\overline{S}\right| \tag{7}$$

where C_s is the Smagorinsky constant varying from 0.1 to 0.8; $\left|\overline{S}\right|$ is the magnitude of $\overline{S}_{ij}$ ($\left|\overline{S}\right| = \sqrt{2\overline{S}_{ij}\overline{S}_{ij}}$) Δ is the length scale for the grid filter and $\overline{S}_{ij}$ is the filtered strain-rate tensor ().

Boundary Conditions of 2dh Models: Boundary conditions commonly considered in 2DH models, include those of the inlet, the outlet and the solid wall. At the inlet boundary, the flow rate must be specified (i.e. $p=p_0$, $q=0$). The free surface elevation, η, would be specified at the outlet boundary. At solid walls, both free slip and no slip boundary conditions may be considered. At no slip conditions, all velocity components are set to zero while at the free slip conditions, just the normal component of the velocity is set to zero. In this study, depending on the flow nature, application of both conditions is possible.

3D RANS Equations: The governing hydrodynamic equations are 3D Navier Stokes equations with the Boussinesq approximation and the incompressible continuity equation. The pressure P is divided into two parts- "hydrostatic pressure" ($-\rho g z$) and "excess pressure" (ρp^*). Therefore we have [24, 25]

$$\frac{\partial u}{\partial t} + \frac{\partial u^2}{\partial x} + \frac{\partial uv}{\partial y} + \frac{\partial uw}{\partial z} + \frac{\partial P^*}{\partial x}$$
$$= \frac{\partial}{\partial x}(\vartheta_t^h \frac{\partial u}{\partial x}) + \frac{\partial}{\partial y}(\vartheta_t^h \frac{\partial u}{\partial y}) + \frac{\partial}{\partial z}(\vartheta_t^v \frac{\partial u}{\partial z}) \tag{8}$$

$$\frac{\partial v}{\partial t} + \frac{\partial uv}{\partial x} + \frac{\partial v^2}{\partial y} + \frac{\partial vw}{\partial z} + \frac{\partial P^*}{\partial y}$$
$$= \frac{\partial}{\partial x}(\vartheta_t^h \frac{\partial v}{\partial x}) + \frac{\partial}{\partial y}(\vartheta_t^h \frac{\partial v}{\partial y}) + \frac{\partial}{\partial z}(\vartheta_t^v \frac{\partial v}{\partial z}) \tag{9}$$

$$\frac{\partial w}{\partial t} + \frac{\partial wu}{\partial x} + \frac{\partial wv}{\partial y} + \frac{\partial w^2}{\partial z} + \frac{\partial P^*}{\partial z}$$
$$= \frac{\partial}{\partial x}(\vartheta_t^h \frac{\partial w}{\partial x}) + \frac{\partial}{\partial y}(\vartheta_t^h \frac{\partial w}{\partial y}) + \frac{\partial}{\partial z}(\vartheta_t^v \frac{\partial w}{\partial z}) \tag{10}$$

$$\frac{\partial u}{\partial x} + \frac{\partial v}{\partial y} + \frac{\partial w}{\partial z} = 0 \tag{11}$$

where u, v and w are the Cartesian components of velocity in the x, y and z directions, respectively (z-axis is in the vertical direction and positive up); t is the time; g is the gravitational acceleration and ϑ_t^h and ϑ_t^v represent the horizontal and vertical eddy viscosities, respectively.

The horizontal eddy viscosity, in this research, is determined by Smagorinsky model as mentioned in the previous section, while the vertical eddy viscosity is computed by *1D k-ε* model which uses transport equation for turbulent kinetic energy, *k* and dissipation of turbulent kinetic energy, *ε*, in the vertical direction. The vertical eddy viscosity from *1D k-ε* model is as follows

$$\vartheta_t^v = C_\mu \frac{k^2}{\varepsilon} \tag{12}$$

In the above expression, C_μ is an empirical coefficient, which is usually a constant equal to 0.09 and k and ε are computed from the following transport equations.

$$\frac{\partial k}{\partial t} = \frac{\partial}{\partial z}(\frac{\vartheta_t^v}{\sigma_k} \frac{\partial k}{\partial z}) + P - \varepsilon \tag{13}$$

$$\frac{\partial \varepsilon}{\partial t} = \frac{\partial}{\partial z}(\frac{\vartheta_t^v}{\sigma_\varepsilon} \frac{\partial \varepsilon}{\partial z}) + C_{1\varepsilon} \frac{\varepsilon}{k} P - C_{2\varepsilon} \frac{\varepsilon^2}{k} \tag{14}$$

where $P = \vartheta_t^v\left((\frac{\partial u}{\partial z})^2 + (\frac{\partial v}{\partial z})^2\right)$ is the production term due to the velocity shear; σ_k, σ_ε and $\sigma_{1\varepsilon}$ are the empirical parameters with constant values equal to 1, 1.3, 1.44 and 1.92, respectively.

Boundary Conditions of 3D Models: Boundary conditions in 3D flow models include those of the inlet, the outlet, the solid walls and the free surface. Velocity distribution in vertical direction used at the inlet is either measured in the laboratory or calculated analytically. At the outlet, the "known water elevation" is the prevailing boundary condition, here it changes to "known excess pressure". Both the free slip and the no slip boundary conditions are used for the channel banks in the variant situations. To find the velocity parallel to the channel bed at the first computational node, the standard wall function law is used.

$$\frac{U_r}{U_*} = \frac{1}{\kappa}\ln(Ey^+) \tag{15}$$

where U_r is the resultant velocity parallel to the bed at the first computational node; $U_* = \sqrt{\frac{\tau_b}{\rho}}$ is the resultant friction velocity; κ is Von Karman constant equal to 0.41; E is the roughness parameter; $y^+ = \frac{U_*Y}{\vartheta}$ is the non

dimensional wall distance; τ_b is the bed shear stress; ρ is density; Y is the normal distance to the wall; and ϑ is the kinematic viscosity.

The major boundary condition along the free surface is the known air pressure. Equating the total pressure to the air pressure acting on the surface (i.e. $z = \zeta$) gives the excess pressure along the free surface as:

$$P_a = -\rho g\zeta + \rho P^* \Rightarrow P^* = \frac{P_a}{\rho} + g\zeta \qquad (16)$$

where P_a is the atmospheric pressure (considered zero here) [23]. The kinematic condition on the free surface, that describes the movement of the water elevation, can be written as

$$\frac{\partial \zeta}{\partial t} + u_s \frac{\partial \zeta}{\partial x} + v_s \frac{\partial \zeta}{\partial y} = w_s \qquad (17)$$

where the subscript s represents the variables located on the surface. In this non-hydrostatic model, the free surface elevation is determined, assuming hydrostatic pressure at top layer cells.

Grid Layout
Grid Layout for the 2DH Model: Small mesh size grids help achieving more precise results in regions of particular interest (the Near Field in our case). In such regions, it is necessary that the computational domain has a longer length than that of the region in question. This is usually either to prevent the undesirable reflections from the boundaries near the model region or to connect the region to the closest known boundary, which may be located very far from the Near Field (hydraulic structures). But, using a fine grid for such a long region will make the computations inefficient. One approach to solve this problem is using an unstructured mesh which enables a finer grid around the Near Field and a coarser one in the Far Field. Since rivers and hydraulic structures have complex geometries and according to what was mentioned above, an unstructured triangular mesh is implemented in the present work to cover the solution domain (Figure 2).

Grid Layout for the 3D Model: To discritize the 3D computational domain in the horizontal plane, the same 2DH unstructured triangular mesh is used. In the vertical direction, the structured grid is employed so as to divide the domain into prisms whose horizontal faces are triangles (meaning the same x and y for each vertex in the vertical direction). This kind of grid layout can fit into complex geometries and makes local mesh refinements possible (Figure 3).
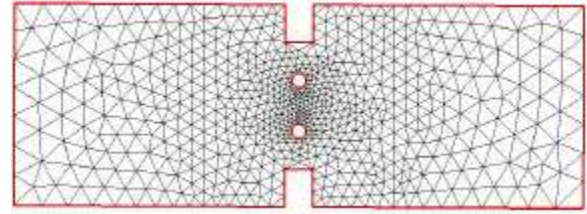

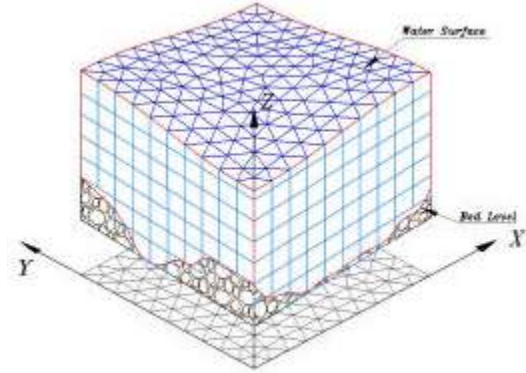Fig. 2: Grid layout of the 2DH calculations

Fig. 3: Grid layout of the 3D calculations (unstructured triangular grids in the horizontal planes and structured grids in the vertical directions).
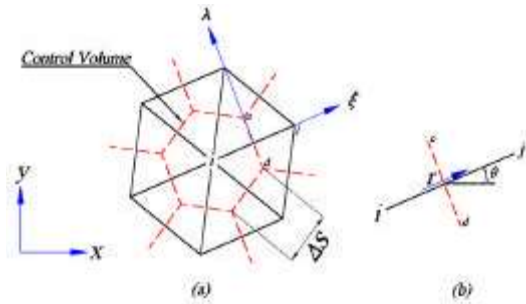

Fig. 4: The control volume for mesh vertex layout (a) and position of r at side ij of the triangular mesh (b)

Numerical Scheme: This section explains the numerical scheme for the solution of 2DH and 3D RANS equations. Equations (1)-(3) and (8)-(11) are solved using the finite volume method.

Numerical Techniques for 2DH Calculations: As mentioned earlier, an unstructured triangular mesh is deployed to discretize the problem domain. Here, using the cell vertex scheme, the centers of the circum-circles of the same elements are connected to construct a control volume for every vertex. In order to determine the components of vector variables normal to each edge of the control volume boundary, the local coordinates ξ and ξ are defined (Figure 4-a).

The present model uses a finite volume fractional step method to solve the governing equations in three steps. The first step, which is a double stage one, solves the advection and diffusion terms in the momentum equations to find the intermediate mass fluxes. In the first stage, p and q are advected using the mass flux field at the previous time step n, to determine the first new intermediate mass flux fields p^{*1} and q^{*1} as

$$\frac{p^{*1} - p^n}{\Delta t} = -\left(\frac{\partial (u\,p)}{\partial x} + \frac{\partial (v\,p)}{\partial y} \right)^n \qquad (18)$$

$$\frac{q^{*1} - q^n}{\Delta t} = -\left(\frac{\partial (u\,q)}{\partial x} + \frac{\partial (v\,q)}{\partial y} \right)^n \qquad (19)$$

The above advection equations are solved using the Fromm second order explicit scheme.

In the second stage, using p^{*1} and q^{*1} and the second order explicit scheme, the diffusion terms are calculated to obtain the second intermediate mass fluxes p^{*2} and q^{*2} as

$$\frac{p^{*2} - p^{*1}}{\Delta t} = \frac{\partial}{\partial x}(\vartheta_t^h \frac{\partial p}{\partial x})^{*1} + \frac{\partial}{\partial y}(\vartheta_t^h \frac{\partial p}{\partial y})^{*1} \qquad (20)$$

$$\frac{q^{*2} - q^{*1}}{\Delta t} = \frac{\partial}{\partial x}(\vartheta_t^h \frac{\partial q}{\partial x})^{*1} + \frac{\partial}{\partial y}(\vartheta_t^h \frac{\partial q}{\partial y})^{*1} \qquad (21)$$

Special techniques for solving advection-diffusion equations on unstructured triangular meshes can be found in Namin *et al.* [27].

The second step uses the semi implicit scheme and solves the friction terms (bed shear stresses) as

$$\frac{p^{**} - p^{*2}}{\Delta t} = -\frac{g p^{**} \sqrt{(p^{*2})^2 + (q^{*2})^2}}{C^2.h^2} \qquad (22)$$

$$\frac{q^{**} - q^{*2}}{\Delta t} = -\frac{g q^{**} \sqrt{(p^{*2})^2 + (q^{*2})^2}}{C^2.h^2} \qquad (23)$$

The third step solves the continuity equation and the remaining terms of the momentum equations simultaneously as

$$\frac{p^{n+1} - p^{**}}{\Delta t} + gh(\frac{\partial \eta}{\partial x})^{n+1} = 0 \qquad (24)$$

$$\frac{q^{n+1} - q^{**}}{\Delta t} + gh(\frac{\partial \eta}{\partial y})^{n+1} = 0 \qquad (25)$$

$$\frac{\partial \eta}{\partial t} + (\frac{\partial p}{\partial x} + \frac{\partial q}{\partial y})^{n+1} = 0 \qquad (26)$$

Equations 24 and 25 can be rewritten as

$$\frac{\partial r}{\partial t} + gh(\frac{\partial \eta}{\partial \xi})^{n+1} = 0 \qquad (27)$$

wher $r = \bar{p}.\cos\theta + \bar{q}.\sin\theta$ is the mass flux component normal to each edge of the control volume boundary; $\bar{p}$ and $\bar{q}$ are the averages of p and q at the endpoints of each side of the triangular mesh (i.e. $\bar{p} = \frac{p_i + p_j}{2}, \bar{q} = \frac{q_i + q_j}{2}$) and θ is the angle between the local coordinates and the Cartesian system (Figure 4-b). The summation of r along all the edges of the control volume at each node causes the variation of water surface elevation inside that node as

$$(\frac{\partial \eta}{\Delta t})_i - \frac{\sum_{m=1}^{k} r_m^{n+1}.\Delta s_m}{Area(i)} = 0 \qquad (28)$$

where *Area(i)* is area of the control volume surrounding the corresponding node, k is the number of edges of the control volume at each node and Δs_m is the length of the mth edge. Equation (28) replaces equation (26). Now, Equations (27) and (28) can be discretized as

$$r_m^{n+1} = r_m^{**} - \frac{\Delta t.g.h}{\Delta \xi}(\eta_j^{n+1} - \eta_i^{n+1}) \qquad (29)$$

$$\eta_i^{n+1} = \eta_i^n - \frac{\Delta t}{Area(i)}\left[\sum_{m=1}^{k}(r_m^{n+1}.\Delta s_m) \right] \qquad (30)$$

Substituting Equation 29 into Equation 30 will result in an equation in which the water surface elevation at each node at time step $n+1$ (η_i^{n+1}) is a function of its surrounding nodes at the same time step. This will end up in n equations with n unknowns (n being the number of nodes in the computational domain). These equations are solved in the present work using an iterative method. Determining η_i^{n+1} for all nodes, p^{n+1} and q^{n+1} are calculated using Gauss's theorem and Equations 24 and 25.

Numerical Techniques for 3d Calculations: As mentioned in Section 3-2, the grid layout for 3D calculations is an unstructured triangular grid in the horizontal plane and a structured one in the vertical direction. P^*, u, v and w are defined at staggered locations as shown in Figure 5.
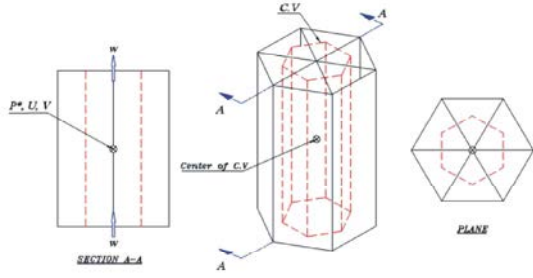
Fig. 5: Definition of variables in a control volume.

In this study, similar to 2DH calculations, a finite volume fractional step method is used to solve the governing equations. Solution procedure consists of two main steps. The advection and diffusion terms of the momentum Equations (8)-(10) are solved in step one. In stage one of this step, the velocity field at the previous time step n is used to advect velocities to determine the new intermediate velocity fields u^*, v^* and w^* as

$$\frac{u^* - u^n}{\Delta t} = -\left[u\frac{\partial u}{\partial x} + v\frac{\partial u}{\partial y}\right]^n - \left[w\frac{\partial u}{\partial z}\right]^* \quad (31)$$

$$\frac{v^* - v^n}{\Delta t} = -\left[u\frac{\partial v}{\partial x} + v\frac{\partial v}{\partial y}\right]^n - \left[w\frac{\partial v}{\partial z}\right]^* \quad (32)$$

$$\frac{w^* - w^n}{\Delta t} = -\left[u\frac{\partial w}{\partial x} + v\frac{\partial w}{\partial y}\right]^n - \left[w\frac{\partial w}{\partial z}\right]^* \quad (33)$$

The velocities are advected in the horizontal plane using the Fromm second order explicit scheme while the Crank-Nicholson implicit scheme is deployed in the vertical direction. In the second stage, using u^*, v^* and w^*, the diffusion terms are calculated to obtain the second intermediate velocities u^{**}, v^{**} and w^{**}, as

$$\frac{u^{**} - u^*}{\Delta t} = \left[\frac{\partial}{\partial x}(\vartheta_t^h \frac{\partial u}{\partial x}) + \frac{\partial}{\partial y}(\vartheta_t^h \frac{\partial u}{\partial y})\right]^* + \left[\frac{\partial}{\partial z}(\vartheta_t^v \frac{\partial u}{\partial z})\right]^{**} \quad (34)$$

$$\frac{v^{**} - v^*}{\Delta t} = \left[\frac{\partial}{\partial x}(\vartheta_t^h \frac{\partial v}{\partial x}) + \frac{\partial}{\partial y}(\vartheta_t^h \frac{\partial v}{\partial y})\right]^* + \left[\frac{\partial}{\partial z}(\vartheta_t^v \frac{\partial v}{\partial z})\right]^{**} \quad (35)$$

$$\frac{w^{**} - w^*}{\Delta t} = \left[\frac{\partial}{\partial x}(\vartheta_t^h \frac{\partial w}{\partial x}) + \frac{\partial}{\partial y}(\vartheta_t^h \frac{\partial w}{\partial y})\right]^* + \left[\frac{\partial}{\partial z}(\vartheta_t^v \frac{\partial w}{\partial z})\right]^{**} \quad (36)$$

The above diffusion equations are solved in the horizontal plane using the second order explicit scheme

and in the vertical direction using Crank-Nicholson implicit scheme.

In the second step, the continuity equation and the remaining term in each momentum equation are solved simultaneously as

$$\left(\frac{\partial u}{\partial x}\right)^{n+1} + \left(\frac{\partial v}{\partial y}\right)^{n+1} + \left(\frac{\partial w}{\partial z}\right)^{n+1} = 0 \quad (37)$$

$$\frac{u^{n+1} - u^{**}}{\Delta t} + (\frac{\partial P^*}{\partial x})^{n+1} = 0 \quad (38)$$

$$\frac{v^{n+1} - v^{**}}{\Delta t} + (\frac{\partial P^*}{\partial y})^{n+1} = 0 \quad (39)$$

$$\frac{w^{n+1} - w^{**}}{\Delta t} + (\frac{\partial P^*}{\partial z})^{n+1} = 0 \quad (40)$$

Approximation of X and Y Derivatives: The x and y derivatives of the horizontal velocities (u, v) at the center of P^* control volume are determined using the Gauss's divergence theorem. According to Figure 6 which displays the horizontal view of the control volume, we can write

$$u_j^{n+1} = u_j^{**} - \Delta t.(\frac{\sum\limits_{m=1}^{nd} P_m^{*n+1}\Delta y_m}{Area_j}) \quad (41)$$

$$(\frac{\partial u}{\partial x})_j^{n+1} = \frac{\sum\limits_{m=1}^{nd} u_m^{n+1}\Delta y_m}{Area_j} \quad (42)$$

$$v_j^{n+1} = v_j^{**} - \Delta t.(\frac{\sum\limits_{m=1}^{nd} P_m^{*n+1}\Delta x_m}{Area_j}) \quad (43)$$

$$(\frac{\partial v}{\partial x})_j^{n+1} = \frac{\sum\limits_{m=1}^{nd} v_m^{n+1}\Delta x_m}{Area_j} \quad (44)$$

where nd is the number of edges of the control volume of each node in plan; Δx_m and Δy_m are the x and y co-ordinate differences of the endpoints of the mth edge (i.e. a, b); u_m^{n+1} and P_m^{*n+1} refer to the average values of u^{n+1} and P^{*n+1} on the mth edge (i.e.

$$u_m^{*n+1} = \frac{u_i^{n+1} + u_j^{n+1}}{2}).$$

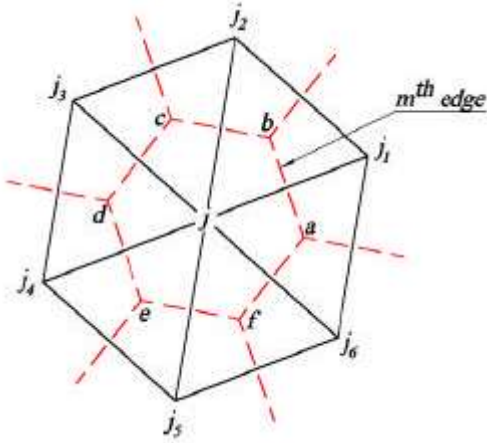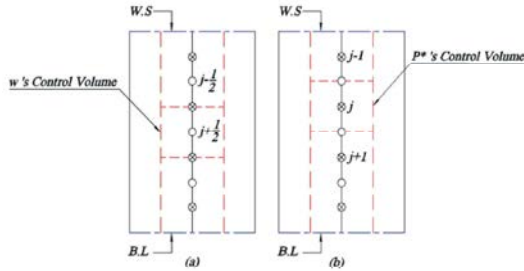As shown in Equations 41 and 43, the values of u^{n+1} and v^{n+1} at each node are defined in terms of P^* at the

Fig. 6: Horizontal view of a control volume

Fig. 7: Side view of w and P^* control volumes

same node (j) and its surrounding nodes (j_1-j_6) at the new time step ($n+1$).

Approximation of the Z Derivative: Figure 7 shows the side view of w and $w^{*n+1}_{j+\frac{1}{2}}$ control volumes. Considering

$$w^{n+1}_{j+\frac{1}{2}} = w^{**}_{j+\frac{1}{2}} + \frac{\Delta t}{\Delta z_j}.(P^{*n+1}_{j+1} - P^{*n+1}_j) \qquad (45)$$

The z derivative of the vertical velocity (w) at the center of P^* control volume (Figure 7-b) is as

$$(\frac{\partial w}{\partial z})^{n+1}_j = \frac{w^{n+1}_{j-\frac{1}{2}} - w^{n+1}_{j+\frac{1}{2}}}{\Delta z_j} = -\frac{\Delta t}{\Delta z_j^2} P^{*n+1}_{j-1}$$

$$+ \frac{1}{\Delta z_j}(\frac{\Delta t}{\Delta z_j} + \frac{\Delta t}{\Delta z_j})P^{*n+1}_j - \frac{\Delta t}{\Delta z_j^2} P^{*n+1}_{j+1} + \frac{1}{\Delta z_j}(w^{**}_{j-\frac{1}{2}} - w^{**}_{j+\frac{1}{2}})$$

$$(46)$$

Solution: As mentioned earlier, the horizontal and vertical velocities are expressed as functions of the excess pressure. Substituting these velocities in the continuity equation will result in a relation in which the excess pressure at each node at time step $n+1$ (P^{*n+1}_j) is a function of the upper, the lower and the surrounding nodes (in plan) at the same time step. This will end up in n equations with n unknowns (n being the number of nodes in the computational domain). These equations are solved in the present work using the line iterative method. Considering time step $n+1$ for the computational nodes in each column in the z direction and time step n for the other nodes, will result in a tri-diagonal matrix system with P^* s as the unknown which can be solved directly. Determining P^* s for all columns in the computational domain, they are replaced with those in the previous iteration. The iterations will continue until the difference between the P^* s in the two successive steps becomes sufficiently small. Having found the excess pressures, the velocities can be calculated using Equations 41, 43 and 45.

Coupled Model: Since the 3D domain (the Near Field) is considered in the present research as a part of a vaster 2DH area (the Far Field), first the whole computational domain is discretized two dimensionally (according to section 3-1). Then, in the 2DH part, which is to be modeled three dimensionally, the same discretization is extended in depth (according to section 3-2). Therefore, the plan of the 3D mesh will coincide with that of the 2DH mesh (Figure 8). This will facilitate the transferring of the parameters calculated from the 2DH model to the 3D model. Now, in order to define a 3D region in a 2DH area, it is necessary to determine the interfacial boundaries at the upstream and the downstream of the 3D region. How the positions of these boundaries are defined will come in the next section.

In this study, the steady state problems have been considered. Hence, in the coupled model, the 2DH equations are first solved for the whole computational domain to converge to the steady state. At the interfacial boundaries, the simulation results of the 2DH calculations are conveyed to the 3D model. For this purpose, the depth averaged horizontal velocities should be distributed in the vertical direction. There are several formulae to distribute the velocity over the flow depth. Logarithmic equations which assume velocity as a logarithmic function over the flow depth are the most frequently used ones. In this research, the following equation, proposed by Van Rijn [28] is used

$$u = \left[\frac{\overline{U}}{\frac{z_0}{h} - 1 + \ln(\frac{h}{z_0})} \right] \ln(\frac{z}{z_0}) \qquad (47)$$
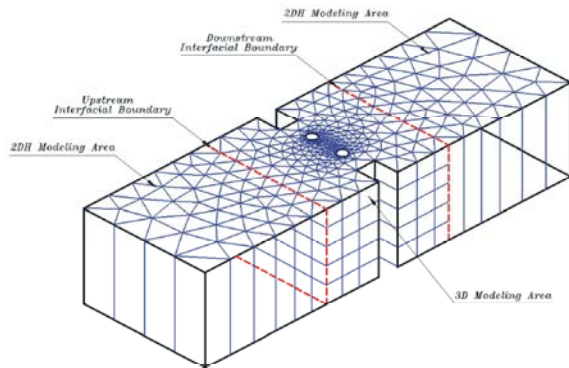
Fig. 8: Grid layout for the coupled model

where z is the vertical distance from the bed, h is the total depth and $z_0 = 0.033.k_s$ (for rough flow regime).

The horizontal velocities, distributed over the flow depth, at the upstream interface and the water surface elevations at the downstream interface, obtained from the 2DH model, are assumed to be constant during the solution of the 3D model. To increase the computational efficiency, the output results of the 2DH model (water surface elevation and horizontal velocities distributed over the flow depth) at nodes located in the 3D domain, are used as the initial guesses (initial conditions) for the 3D model. After determining the boundary and the initial conditions of the 3D model, the flow in the Near Field region is simulated by the 3D model using the procedure explained in section 4-2.

Location of the Interfacial Boundaries: In the coupled model, it is necessary to determine the position of interfacial boundaries at the upstream and the downstream of the 3D region to define the 2DH and 3D areas. As mentioned, the main objective of this research is the accurate prediction of flow around river hydraulic structures; so, the distance from the interfacial boundaries to the flow inlet and outlet (2DH boundaries) should be enough to minimize undesirable reflections from these boundaries. Furthermore, the interfacial boundaries should be far enough from the river hydraulic structures so that the shallow water conditions prevail at the interfacial boundaries. In other words, it is more desirable that the interfacial boundaries are located in the places where vertical velocities are small and, therefore, bathymetry variations are smooth.

Model Validation: Validation of the developed 2DH, 3D and coupled models are dealt with in this section. For the 2DH model we consider one test case and for the other models, two test cases.

Validation of the 2DH Flow Model: To validate the 2DH model, the results of the A1 test carried out by Rajaratnam and Nwachukwu [29] on flows near a spur dike are used. They used a thin aluminum plate as a spur dike fixed perpendicular to the side of a long rectangular channel. Their flume had a length of 37m, a width of 0.9m, a depth of 0.76m, smooth bed and sides. The spur dike, projecting above surface of water, was 3mm thick and 152mm long. H and U_0 (water depth and flow velocity) in the A1 test were 0.189m and 0.253m/s, respectively.

To simulate their flow conditions numerically, we considered a 20m×.9m computational domain for which the upstream and downstream boundaries were located respectively 3m and 17m away from the spur dike. Discretization of this domain resulted in 17549 triangles. Flow flux at the upstream boundary and the water depth at the downstream boundary were 0.047817m^2/s and 0.189m, respectively. Free slip boundary condition was applied at the channel walls. The calculated resultant velocity profiles at $y/b=3$ and $y/b=4$ (b being the length of the spur dike), normalized by $U_0=0.253$m/s, are shown in Figure 9. Comparison of the numerical results and the experimental data shows good agreement.

Validation of the 3D and the Coupled 2DH-3D Flow Models: In order to validate the 3D flow model and verify the capability, accuracy and efficiency of the proposed coupled model, both models were used to simulate flow around a spur dike and a bridge pier which are considered to be typical river hydraulic structures. For each structure one experimental test case was carried out, the parameters of which are summarized in Table 1.

To compare the efficiency and accuracy of the coupled 2DH-3D model with those of the 3D model, the same computational domain was used for both models.

Flow Simulation Around a Cylindrical Pier: For the first test case of the 3D and the coupled 2DH-3D models, the experimental results obtained by Ahmed and Rajaratnam [30] (Experiment C2R) were considered for the sake of comparison. Their experiments were conducted in a 20m long and 1.22m wide flume; a 0.089m diameter cylinder was

Table 1: Geometric parameters and tests conditions

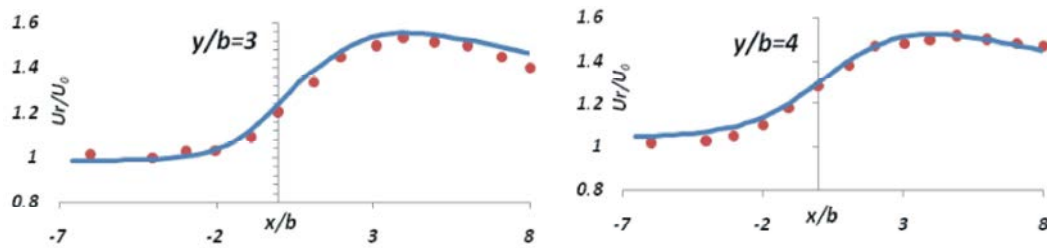| Test case	Structure	Flume dimensions (length/width)	Flow depth (m)	Mean approaching flow velocity (m/s)	Dimensions of structure (length/thickness or diameter)
1	Cylindrical pier	20 m/1.22 m	0.182	0.2927	0.089 m
2	Spur dike	32.4 m/2.5 m	0.23	0.3478	0.25 m/0.05 m

Fig. 9: Computed resultant velocity profiles (solid lines) and experimental data (closed circles) at (a) y/b=3 and (b) y/b=4 (x/b=0 is the spur dike position).
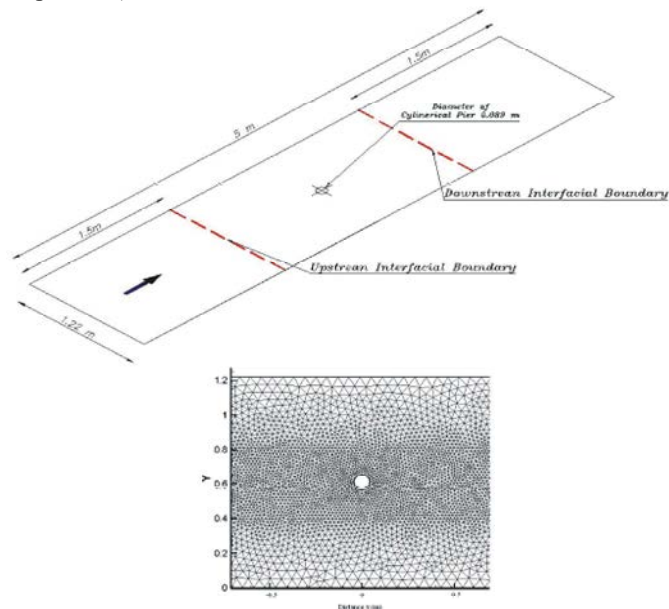

Fig. 10: Plan view of the whole computational domain and positions of the interfacial boundaries (a) and grid around cylindrical pier in the x-y plane (b)
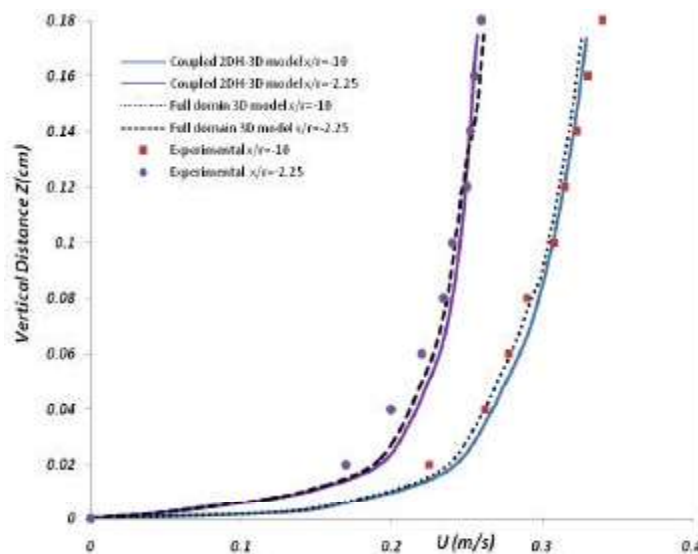

Fig. 11: Vertical distribution of the streamwise velocity (u) obtained from numerical models and experiments (x/r =0 is the pier position).
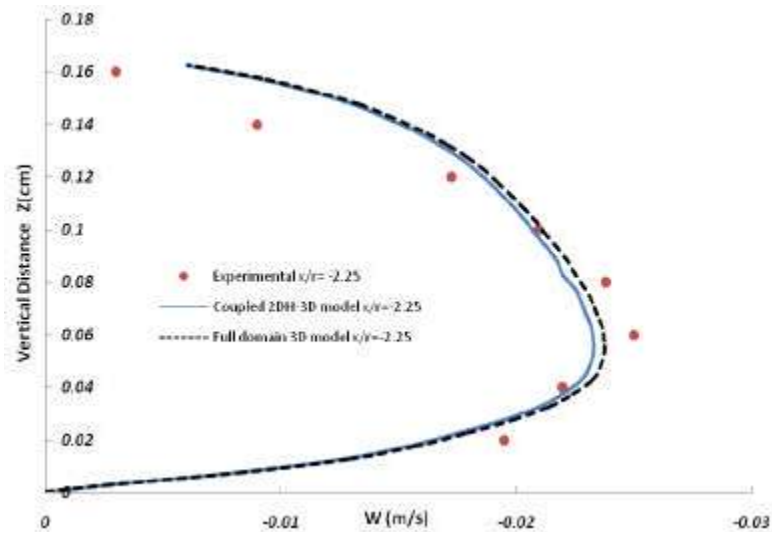
Fig. 12: Vertical distribution of the vertical velocity (w) obtained from numerical models and experiments
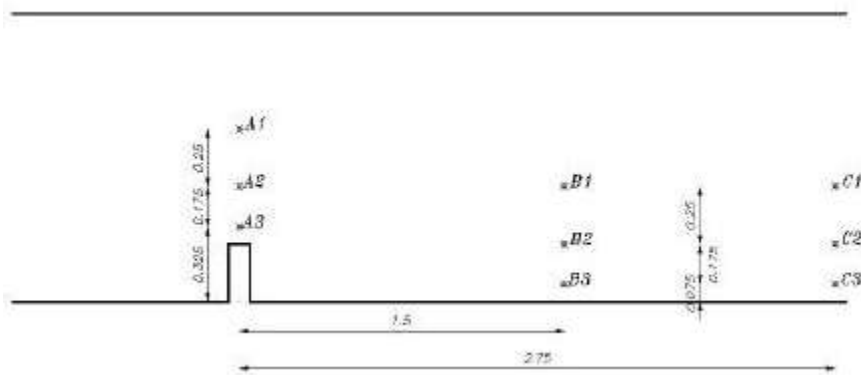

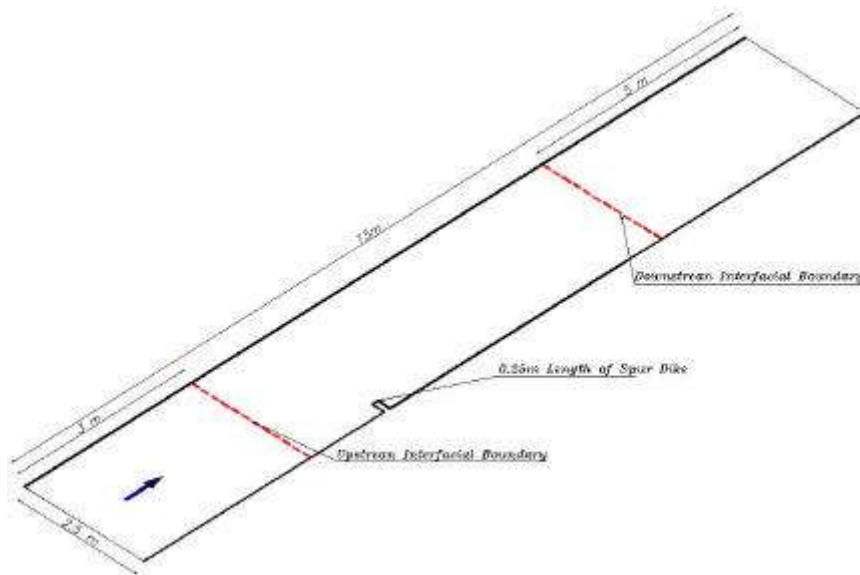Figure 13. Points where velocities were measured.

Fig. 14: Plan view of the whole computational domain and positions of the interfacial boundaries
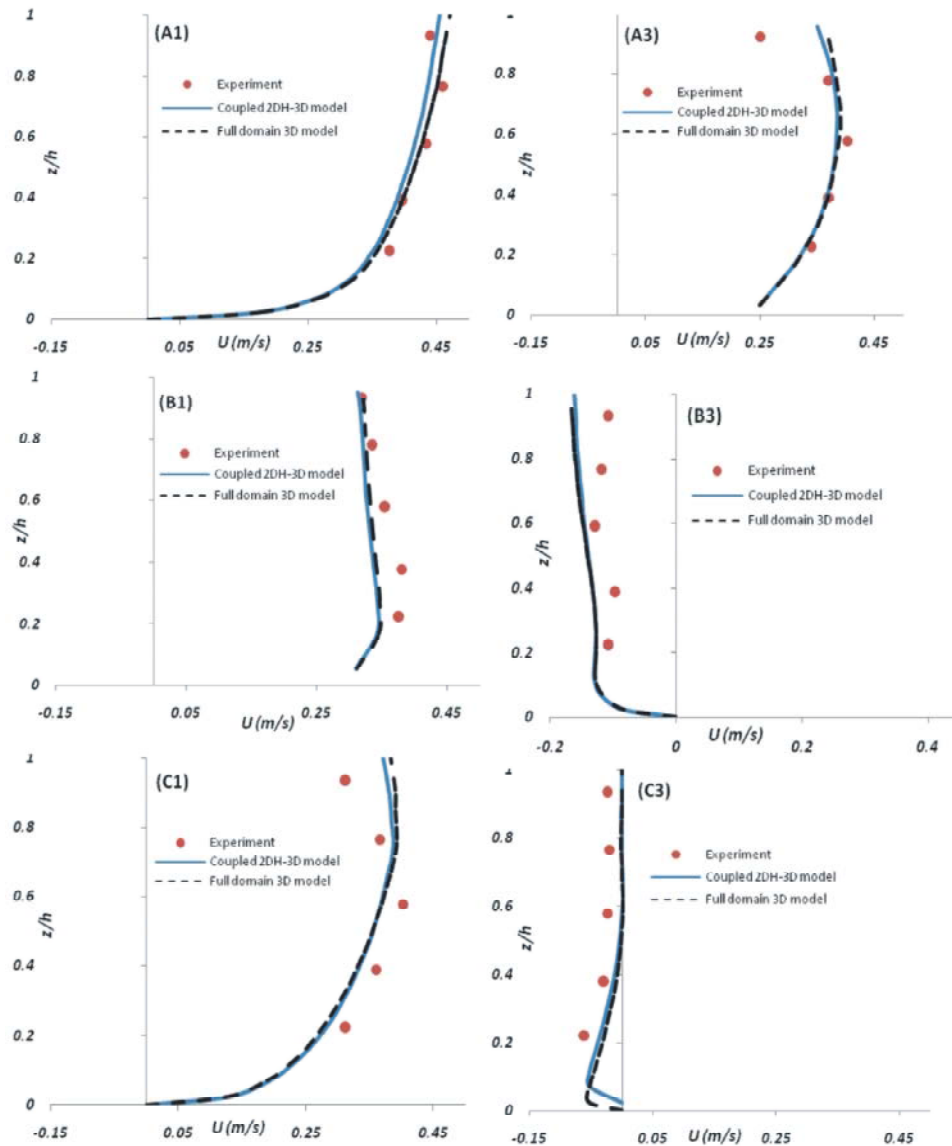
Fig. 15: Comparisons of numerical results of the 3D and the coupled 2DH-3D models (solid and dashed curves) for streamwise velocity profiles with the experimental data (closed circles) at locations A1, A3, B1, B3, C1 and C3

used as a model for the bridge pier. The approaching flow velocity and the water depth were 0.2927 m/s and 0.182m, respectively.

Our computational domain was 5m by 1.22m and the pier was located in the middle. First, the whole computational domain was simulated by the 3D elements and the results were compared with the experimental data. Then the 2DH-3D coupled model was used for the same computational domain. In the coupled model, the area around the pier was simulated by 3D modeling and the rest of the domain by the 2DH model. According to the flow conditions, the interfacial boundaries were assumed

at 1m upstream and downstream of the pier as shown in Figure 10-a. In order to investigate the flow details around the pier, a finer mesh was used (Figure 10-b).

The 3D and the coupled 2DH-3D model results were compared with the experimental data of the vertical distribution of the streamwise velocity (u) at different locations upstream of the pier as shown in Figure 11; the comparison shows good agreement.

The vertical distribution of the vertical velocities (w) upstream of the pier, obtained from the experiments and the models, were compared (Figure 12). They are in great agreement.
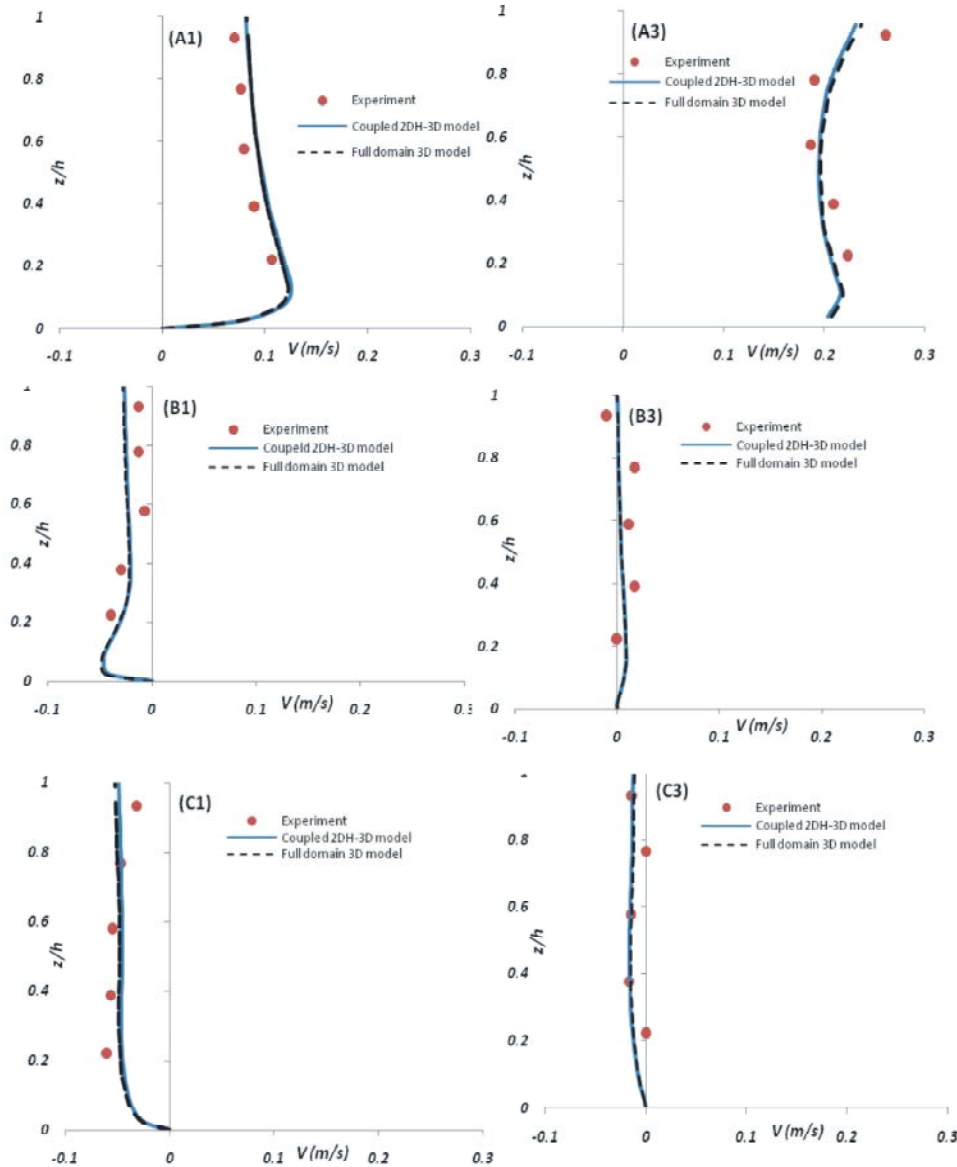
Fig. 16: Comparisons of numerical results of the 3D and the coupled 2DH-3D models (solid and dashed curves) for transverse velocity profiles with the experimental data (closed circles) at points A1, A3, B1, B3, C1 and C3

Figures 11 and 12 clearly show that the difference between the results of the 3D flow simulation for the whole computational domain and the coupled 2DH-3D model is very small. However, the important point is that the computation time needed for the coupled model is only about 6% of that needed for the 3D modeling of the whole computational domain.

Flow Simulation Around Non-Submerged Spur Dike: For the second test case, results of the 3D and the coupled models were compared with those of one of the experiments done at Franzius Institute in Hannover (reported by Muller and Schwarze [31]). This experiment was carried out in a 32.4m by 2.5m channel having smooth vertical walls. The flow rate and the water depth were $0.2m^3/s$ and 0.23m respectively. The spur dike was 0.25m long (along channel width) and 0.05m thick. Points where velocities were measured are shown in Figure 13. Mayerle *et al.* [6] too applied these experimental data to verify their numerical model.

In this case, our computational domain was considered to be 15m by 2.5m and the spur dike was located 5m downstream of the inlet. Similar to the previous test case, first the whole computational domain was

simulated by 3D elements and the results were compared with the experimental data. Then, the 2DH-3D coupled model was implemented for the same computational domain.

For the coupled model, the area around the spur dike was simulated using 3D modeling and the rest by using the 2DH model. Interfacial boundaries were assumed at 2m and 5m upstream and downstream of the spur dike, respectively (Figure 14).

Vertical distribution of the streamwise and transverse velocities at points A1, A3, B1, B3, C1 and C3, obtained from the 3D and the coupled models, have been compared with those of the experiment as shown in Figures 15 and 16. These Figures show that the measured and the computed velocities from the 3D and the coupled 2DH-3D models agree satisfactorily.

It is worth mentioning that the computational time of the proposed coupled 2DH-3D flow model is only 8% of that of the normal 3D model used for the whole domain. This means that the proposed model reduces the computational time considerably.

Figure 15. Comparisons of numerical results of the 3D and the coupled 2DH-3D models (solid and dashed curves) for streamwise velocity profiles with the experimental data (closed circles) at locations A1, A3, B1, B3, C1 and C3

Figure 16. Comparisons of numerical results of the 3D and the coupled 2DH-3D models (solid and dashed curves) for transverse velocity profiles with the experimental data (closed circles) at points A1, A3, B1, B3, C1 and C3

CONCLUSIONS

To simulate flow around river hydraulic structures, a coupled 2DH-3D numerical model has been proposed in this research. 2DH models can simulate the overall pattern of river flows with acceptable accuracy while strong three dimensional flows caused by the downward flow along the upstream face of the river hydraulic structures, make the implementation of a full 3D model necessary around such structures. In the proposed coupled model, the full 3D modeling has been used for the area surrounding river hydraulic structures and the 2DH model for the rest of the channel. The latter has been based on an unstructured triangular mesh while the former has been formulated on an unstructured grid in the horizontal plane and a structured grid in the vertical direction. Both models have taken advantage of the finite volume fractional step method to discretize the governing equations. At the connection boundaries between the 2DH and the 3D

areas, the simulation results of the 2DH calculations have been transferred to the 3D model using proper relations. The results of the 2DH, the 3D and the coupled 2DH-3D models have been verified by several test cases with good satisfaction.

- The proposed coupled model provides several advantages as follows:

- It can considerably reduce the computational time and increase the computational efficiency (time consumed by this model to simulate flow around two typical river hydraulic structures was only about 7% of that taken by normal 3D for the whole computational domain).
- It can adopt complicated boundaries and be refined in areas where more resolution is necessary because it takes advantage of an unstructured grid to solve the numerical algorithms.
- In the present non-hydrostatic 3D model, the elevation of the free surface is defined by an assumed hydrostatic pressure at the top layer cells; hence, the variations of the free surface elevation can occur only in that layer. While converging to the steady state, the difference between the maximum and the minimum free surface elevations at successive time steps may be larger than that in the final results. This may cause formation of a thick layer at the top cells– hence a reduction in accuracy. By using the water surface elevation, obtained from the 2DH model, as the initial guess for the 3D portion of the coupled model, the thickness of the top layer can be reduced noticeably.
- Since in practice there is no need for 3D simulation of areas located far from the river hydraulic structures, the proposed coupled 2DH-3D model is considered quite suitable for large scale modeling.

REFERENCES

1. Chen, N.S. and C.H. Li, 1989. Numerical solution of the flow around a spur dike with k-ε turbulent model. J. Nanjing Hydraulic Research Institute, 3: 11-23.
2. Tingsanchali, T. and S. Maheswaran, 1990. 2-D depth-averaged flow computation near groyne. J. Hydraulic Engineering (ASCE), 116(1): 71-86.
3. Molls, T. and M.H. Chaudhry, 1995. Depth-averaged open-channel flow model. J. Hydraulic Engineering (*ASCE*), 121(6): 453-465.

4. Molls, T., M.H. Chaudhry and K.W. Khan, 1995. Numerical simulation of two-dimensional flow near a spur dike. J. Advance in Water Reso., 118(4): 227-236.

5. Jia, Y., S.Y.Y. Wang and Y. Xu, 2002. Validation and application of a 2D model to channels with complex geometry. International J. Computational Engineering Sci., 3(1): 57-71.

6. Mayerle, R., F.M. Toro and S.S.Y. Wang, 1995. Verification of a three-dimensional numerical model simulation of the flow in the vicinity of spur dikes. J. Hydraulic Res., 33(2): 243-256.

7. Ouillon, S. and D. Dartus, 1997. Three-dimensional computation of flow around groyne. J. Hydraulic Engineering (ASCE), 123(11): 963-970.

8. Tseng, M.H., C.L. Yen and C.S. Song, 2000. Computation of three-dimensional flow around square and circular piers. International J. for Numerical Methods in Fluids, 34: 207-227.

9. Kamil, H.M. and K.O. Ali, 2002. Simulation of flow around piers. J. Hydraulic Res., 40(2): 161-174.

10. Kimura, I. and T. Hosoda, 2003. A non linear k-ε model with realizability for prediction of flows around bluff bodies. International J. For Numerical Methods in Fluids, 42: 813-837.

11. Zhou, Y., M. Michiue and O. Hinokidani, 2004. Study on flow characteristics around the non-submerged spur dike. J. Hydraulic Engineering (In Chinese), 8: 46-53.

12. Salaheldin, T.M., J. Imran and M.H. Chaudhry, 2004. Numerical modeling of three-dimensional flow field around circular piers. J. Hydraulic Engineering (ASCE), 130(2): 91-100.

13. Roulund, A., B.M. Sumer, J. Fredsoe and J. Michelsen, 2005. Numerical and experimental investigation of flow and scour around a circular pile. J. Fluid Mechanics, 534: 351-401.

14. Nagata, N., T. Hosoda, T. Nakato and Y. Muramoto, 2005. Three-dimensional numerical model for flow and bed deformation around river hydraulic structures. J. Hydraulic Engineering (ASCE), 131(12): 1074-1087.

15. Xuelin, T., D. Xiang and C. Zhicong, 2006. Large eddy simulation of three dimensional flows around a super dike. J. Tsinghua Science and Technol., 11(1): 117-123.

16. Xuelin, T., 2007. Experimental and numerical investigations on secondary flows and sedimentations behind a super dike. J. Hydrodynamics, Series B, 19(1): 23-29.

17. McCoy, A., G. Constantinescu and J. Weber, 2008. Numerical investigation of flow hydrodynamics in a channel whit series of groynes. J. Hydraulic Engineering (ASCE), 134(2): 157-172.

18. Yazdi, J., H. Sarkardeh, H.M.D. Azamatulla and A. Ghani, 2010. 3D simulation of flow around a single spur dike with free surface flow. International J. River Basin Manage., 8(1): 55-62.

19. Miglio, E., S. Perotto and F. Saleri, 2005. Model coupling techniques for free surface flow problems: Part . Nonlinear Analysis, 63: 1885-1896.

20. Fang-li, Y., Z. Xiao-feng and T. Guang-ming, 2007. One and two-dimensional coupled hydrodynamics model for dam break flow. J. Hydrodynamics, 19: 769-775.

21. Mahjoob, A. and R. Ghiassi, 2011. Application of a coupling algorithm for the simulation of flow and pollution in open channels. World Applied Science J., 12(4): 446-459.

22. Namin, M.M. and R.A. Falconer, 2004. An efficient coupled 2-DH and 3-D hydrodynamic model for river and coastal applications. In Proceeding of the 6th International Conference on Hydroinformatics, Liong, Phoon and Babovic.

23. Zounemat, K.M. and S.R. Sabbagh-Yazdi, 2010. Coupling of two- and three-dimensional hydrodynamic numerical models for simulating wind-induced currents in deep basins. Computers and Fluids, 39: 994-1011.

24. Badiei, P., M.M. Namin and A. Ahmadi, 2008. A three-dimensional non-hydrostatic vertical boundary fitted model for free-surface flows. International Journal for Numerical Methods in Fluids, 56: 607-627.

25. Namin, M.M., 2003. A fully three dimensional non hydrostatic free surface flow model for hydro environmental predictions. *Ph.D. Thesis*, Cardiff School of Engineering, Cardiff University.

26. Namin, M.M., B. Lin and R.A. Falconer, 2001. An implicit numerical algorithm for solving non-hydrostatic free surface flow problems. International Journal for Numerical Methods in Fluids, 35: 341-356.

27. Namin, M.M., B. Lin and R.A. Falconer, 2004. Modeling estuarine and coastal flows using an unstructured triangular finite volume algorithm. J. Advances in Water Reso., 27: 1179-1197.

28. Van Rijn, L.C., 1993. Principles of sediment transport in rivers, estuaries and coastal seas. Aqua Publications, Amsterdam, the Netherlands.

29. Rajaratnam, N. and B.A. Nwachukwu, 1983. Flow near Groin-like structures. J. Hydraulic Engineering (ASCE), 109(3): 463-480.

30. Ahmed, F. and N. Rajaratnam, 1998. Flow around bridge piers. J. Hydraulic Engineering, 124(3): 288-300.

31. Muller, K.D. and H. Schwarze, 1990. Model investigation of 3-d current conditions in harbor entrances. Proceedings of the National Conference (In ASCE), 2: 879-884.